Lab 4: Infrared Observations of the NGC 1333 Star Forming Region

Andy Friedman [1,2]

November 13, 2001

ABSTRACT

In this report, we discuss near infrared K, H, and J observations of the NGC 1333 Star Forming Region in the constellation Perseus, using the Leuschner Observatory 30-inch telescope and infrared camera. We observed our star cluster, a control field, and our standard stars on the same night under nearly identical observational conditions. After calibrating our data, (flat fielding, dark subtracting, sky subtracting), we assembled our data into a mosaic for each band, and combined the bands to create false color RGB images of our cluster and control field. We then performed differential photometry on the entire image using a convolution technique and obtained standard magnitudes for only the brightest stars that could be seen in all three bands.[1] This turned out to be 45 stars for our cluster and 14 in our control field. To correct for reddening, we assembled a $(J-H)$ vs $(H-K)$ color-color diagram and calculated the reddening for each Main Sequence (M.S.) star, finding average reddening values of $A_V \approx 9.5$ mag toward our cluster and $A_V \approx 1.7$ mag toward our control field, indicating that the cluster suffered from significantly greater extinction by interstellar dust. After correcting for reddening for only the M.S. stars, we constructed the reddening corrected luminosity function for our cluster and control field in all 3 bands. The M.S. stars we performed photometry on in our cluster ranged in brightness from $m \approx 5$ in all bands to $m \approx 13$ in K and H, and $m \approx 14$ in J. For our control field, the 12 M.S. stars we did photometry on ranged in brightness from $m \approx 9$ to $m \approx 12$ in all bands. We finally constructed a M_k vs. $(J-K)$ color-magnitude diagram for both the reddening-corrected M.S stars in our cluster and the non-M.S. stars which had not been corrected for reddening. We then found the mass of the faintest M.S. star we did photometry on from its measured spectral type, $K0$, obtaining $M \approx 0.67 M_\odot$. We then found an upper limit for the age of the cluster by finding the spectral type of the most massive M.S. star on the diagram that had not yet left the Main Sequence, and then calculating its age.[2] This gave us an upper limit for the age of the cluster of $\approx$ 19 million years, consistent with the age of 1-2 million years, found by Lada et al. (1996).

---

[1] e-mail: friedman@ugastro.berkeley.edu

[2] Lab Group: Lee, Jim, Christina, and Lindsey

[1] This introduces a bias which we must be aware of, as we did not perform photometry on the faintest stars in the image that only appeared in only 1 or 2 of the bands.

[2] In calculating the lifetime of the cluster, we assumed an α of 3.5 for the mass-luminosity relationship for Main Sequence Stars ($L \propto M^\alpha$). More details can be found later in the report.

1. Introduction: The Basics of Star Formation and Evolution

Stars form out of clouds of gas and dust that collapse under gravity. In NGC 1333 and in other star forming regions, infrared observations offer a glimpse at this process in action. Jeans was the first to show that clouds of a certain mass and size will be unstable against gravitational collapse. His criteria are given by the Jeans Mass M_J and Jeans Radius R_J, shown below:

$$M_J \approx \left(\frac{5kT}{G\mu m_p}\right)^{3/2}\left(\frac{3}{4\pi\rho_o}\right)^{1/2} \qquad R_J \approx \left(\frac{15kT}{4\pi G\mu m_p\rho_o}\right)^{1/2} \tag{1}$$

where T is the temperature of the cloud, ρ_o is the density, μ is the mean molecular weight of the gas, k is Boltzmann's constant, G is Newton's gravitational constant, and m_p is the proton mass. Gas clouds with masses greater than M_J and radii greater than R_J can collapse, and will often fragment into regions of higher density that eventually become stars.

During the collapse phase, energy from gravitational contraction is the only power source which provides a gas pressure which can fight gravitational collapse and keep the star in pseudo hydrostatic equilibrium. In this phase, the star is called a Pre-Main Sequence or (PMS) star. The virial theorem tells us that when a star contracts, half of the gravitational energy used goes into heating up the star and half of it gets radiated. Thus the star heats up and brightens as it contracts. The timescale over which the star can survive this way powered only by gravitational contraction is given by the Kelvin-Helmholtz time t_{KH}. For a spherical star of constant density, mass M, and final radius R, and luminosity L, t_{KH} is given by:

$$t_{KH} \approx \frac{1}{L}\frac{3}{10}\frac{GM^2}{R} \tag{2}$$

This assumes the initial radius $R_i >> R$, and that the star's luminosity L remains constant during the collapse. For the sun, $t_{KH} \approx 10^7$ years. As this timescale is much too short to be consistent with the age of the earth from the radioactive dating of rocks (not to mention the evolution of human life), astronomers such as Bethe recognized that there must me some other energy generation mechanism for stars. This mechanism turns out to be nuclear fusion in the star's core.

When the core of a collapsing cloud heats up enough, it can start fusing hydrogen to helium. Once such nuclear reactions have begun, the star enters the Main Sequence (M.S.), where it resides for much of its life. Low mass stars burn their fuel at a slow rate and live a long time on the M.S. The sun's M.S. lifetime is $\approx 9 \times 10^9$ years, for example. High mass stars, by contrast live shorter lives. Even though they begin with more fuel, they burn it at a disproportionate rate. More detailed calcualtions of the mass-luminosity relationship and the lifetimes of M.S. stars will be discussed later in this report when we estimate the age of our cluster. When a star has exhausted the hydrogen in its core, it is on its way towards leaving the Main Sequence. Most such stars will become a red giant or a red supergiant, depending on their initial mass. A discussion of the physics of post M.S. stars can be found in CH. 13 of Carroll & Ostlie. In a young star cluster such as NGC 1333, we can see stars throughout nearly all stages of evolution, most notably PMS stars, M.S. stars, and a few Giant stars that have left the M.S.

2. Interstellar Extinction

Gas and dust particles in interstellar space absorb photons coming from stars, making those stars appear dimmer. This is the phenomenon of interstellar extinction. It is also called reddening since dust grains preferentially absorb blue light, making the object appear redder. To correct for this and determine the star's true apparent brightness, we must understand a bit about the physics of dust. For a beam of light of initial intensity I_o passing through a dusty region of unit area A =1, and length dl, the infinitesimal drop in intensity I is given by $dI/I = -dA = n\sigma dl$, where n is the number density of dust grains and σ is the effective interaction cross section of each dust grain. Solving this differential equation for I, in terms of the initial beam intensity I_o, we find:

$$I = I_o e^{-\tau} = I_o e^{-\int n\sigma dl} = I_o e^{-n\sigma l} \tag{3}$$

where $\tau = \int n\sigma dl = n\sigma l$ is the optical depth. Given τ, we define the extinction in magnitudes by:

$$A = -2.5\ log\left(\frac{I}{I_0}\right) = 1.086\tau \tag{4}$$

If we denote A_V as the extinction in the visible band, from the table below, we can see that dust affects different wavelengths of light differently. For example, the near-infrared wavelengths K, H, and J are significantly less affected by dust than visible light. This makes them optimal wavelengths in which to observe star forming regions where we expect the presence of significant amounts of dust which can obscure much of the process we are interested in observing.

Band	Wavelength (nm)	A/A_V
V	551	1.000
J	1220	0.282
H	1630	0.175
K	2190	0.112

Table 1: *The A in A/A_V can stand for the extinction in any band, i.e. for $A_V, A_K, A_H, or A_J$ for the bands shown here. Note that the visible band is the reference point as evidenced by the fact that for visible light, $A/A_V = A_V/A_V = 1.000$. This table will be useful later in calculating reddening.*

So if we observe a star in the K filter, for example, with magnitude K (or equivalently, m_K), the magnitude corrected for interstellar extinction is denoted by K_o and is given by:

$$K_0 = K - A_k = K - 0.112A_V \tag{5}$$

So if we determine A_V for a given star in our cluster, we can correct for reddening in any near infrared wavelength. This model assumes the physics of dust grains is the same throughout all of space, which may not be the case. If the model fails to explain observations, it might suggest the existence of some new variety of "superdust". Luckily for us, NGC 1333 is a well observed region and we can trust that our dust model is adequate for our purposes.

3. Obtaining K, H, and J Infrared Images

We used our previous experience with the Leuschner telescope and infrared camera to take images of our star cluster NGC 1333 in the K, H, and J bands. We observed both our cluster and a chosen control field, taking a 7x7 raster pattern for a total of 49 images each in each band. We took 10s exposures for all science frames, giving us a maximum effective exposure time in the center of our raster pattern of 490s or roughly, 8.17 minutes. We then observed our standard stars (3 infrared standards in the field SAO056596) under nearly identical conditions and took a 3x3 raster pattern for a total of 9 images in each band. We took flats at twilight and darks throughout, then calibrated the raw data using the previous techniques of flat fielding, dark subtraction, and a slightly improved sky subtraction technique. We also made refinements to our bad pixel mask by identifying a few nasty bad pixels that had eluded us in our previous attempts.

As in the previous lab, a plot of Elevation vs. LST for NGC 1333 is shown below which tells us when we can observe our cluster. This object required us to spend many late nights and mornings in the lab as evidenced by the "graveyard shift" time window shown below.

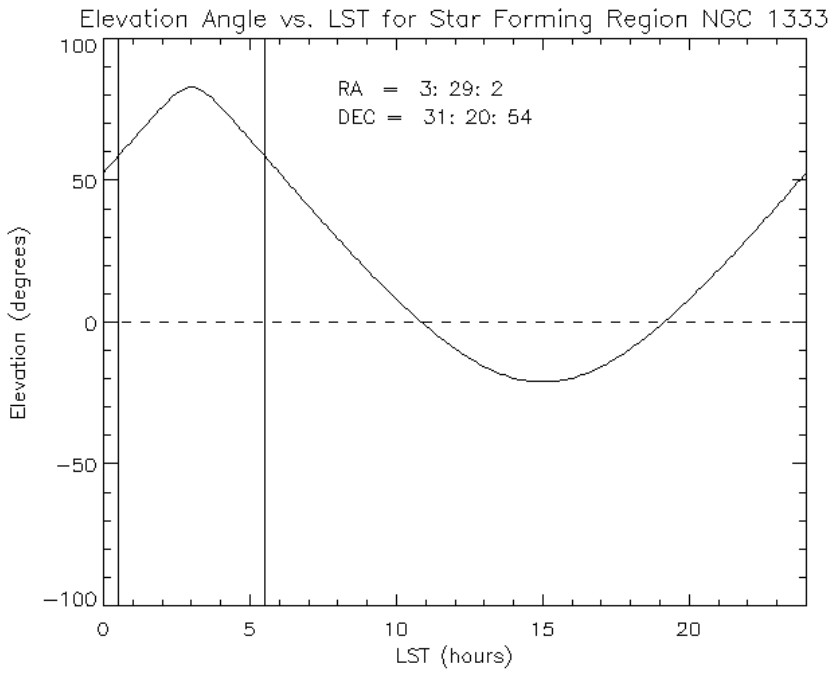

Fig. 1.— This plot tells us when our object will be observable at night. For NGC 1333 we can begin observing the field at an LST of roughly 0.5 hours, or a bit before 1:00am in Pacific Standard Time. Our hour angle limit gives us an observation window of roughly 5 hours in which to take data including darks, sky, control field, standard stars, and science images. Flats can be taken at twilight or before dawn.

3.1. Raster Scripts

With several hundred images to take, practicality required us to write scripts which would raster the telescope and take all the desired images. This task was accomplished thanks primarily to the work of Jim Brennan, the champion observer of our group. As in previous labs, one purpose of rastering is to ensure that every bit of sky will see a good pixel at least once. Bad pixels stay in the same place on our camera, so when we raster, we effectively move the sky around and allow stars to fall on different pixels. The second purpose of rastering here was simply to take multiple images which we would eventually combine into a mosaic to increase the effective exposure time of the cluster. Rastering also allows us to image a wider field of view than the 5.8' x 5.8' of our camera alone, although the effective exposure time toward the outer regions is comparatively minimal. NGC 1333 has a field of view of 15' x 15', which is much too large for us to fully image, so we contented ourselves to focusing on an interesting region in the northeast corner.

In our attempt to observe our Cluster, Control Field, and Standards as identical observational conditions as possible (necessary for relative photometry) we wanted to place them fairly near each other in the sky, so we could raster between them in a time scale short enough to avoid changing detector temperature and extreme variations in sky brightness. Since NGC 1333 is located at RA: 3 29 02.0 Dec: +31 20 54.0 we used the infrared standard stars, SAO056596, that are located at RA: 3 38 08.3 Dec: +35 10 52 close by. The control field was also located nearby at roughly 0.4 degrees in RA to the West. We used the median of our cluster to find our sky value and noticed large sky variation over a time scale of a few minutes, which we had to correct for.

As in the previous lab, the standard stars are observed to allow us to eventually perform differential photometry. The purpose of Control Field is two fold. First off we could estimate our sky value from the control field if our cluster field is too crowded for the median to pick out only the sky. Secondly, we use it as a comparison field to test whether the "cluster" is actually a cluster. We can do this by comparing the mean star brightness in the control filed and cluster images, or we can apply the more statistically rigorous Komolgorov-Smirnov test. However, using a sophisticated quantitative test to answer the largely qualitative question, "Is my cluster different from my control field?" is not extremely useful considering that this does not give you much more information than a visual inspection of the images from which it is easy enough to say, gee, there are a lot more stars in this image than in the control field, so its probably a cluster.

Filter	Band Width Range (μm)
J	1.783 to 1.487
H	1.328 to 1.165
K	2.302 to 1.991
Aluminum Plug	—

Table 2: *The Band Width Ranges for the K, H, and J filters are displayed above. We also used the Aluminum plug on the filter wheel to take dark images which require the blockage of outside light.*

3.2. Flat Fields, Dark Subtraction, and Sky Subtraction

Using techniques from previous labs, we took 49 dark current images with the same exposure time as our science exposure (t = 10s) and combined them to make super dark image $Dark(x, y)$ with an error well below 1%. We took 25 flats at twilight (each 10s exposures) and constructed an array of pixel by pixel gain variations. Combining them to make the super flat array $Flat(x, y)$ gave an error from added variances well below 1%. We ended up using the median of our cluster field as our sky value. We were wary that our cluster might be too crowded or have too high a nebulosity such that the median might reflect the presence of stars and not the sky alone, but we found it was adequate and used it rather than the control field to find our median sky. We finally constructed a super sky image $Sky(x, y)$ by taking a pixel by pixel median of the stacked sky images. To calibrate each of the 49 science images in each band $Science(x, y)[i]$, we used the following procedure.

$$S_{calibrated}[i] = \left(\frac{Science(x,y)[i] - Dark(x,y)}{Flat(x,y)}\right) - \left(\frac{Sky(x,y) - Dark(x,y)}{Flat(x,y)}\right) \tag{6}$$

We performed this process for each rastered image. When we constructed a mosaic (described in the next section) using only the above steps, we noticed light and dark bands across the bottom and top of our final mosaic. We realized that these reflected significant changes in sky brightness in our science image as we completed our raster pattern, sweeping out rows from right to left and left to right. The time scale for large variations in sky was on the order of a couple of minutes, much shorter than for our entire raster pattern, and it was clear that our 49 science images had highly varying backgrounds when we displayed them side by side all with the same tv scaling. To correct for this, since the sky value is simply arbitrary, we applied the final correction to each image.

$$S_{final}[i] = S_{calibrated}[i] - median(S_{calibrated}[i]) \tag{7}$$

Subtracting off the median of each corrected science image from itself adequately compensated for sky brightness changes from image to image, as evidenced by the remarkable background uniformity in our final mosaic images.

3.3. Bad Pixel Mask

We had previously constructed a bad pixel mask, but it became evident that we were missing a few nasty pixels as they continually marked out clear 7 x 7 patterns in our early mosaics. To remove them, we tried to make the bad pixel program more robust and removed particularly evil pixels by hand when necessary. The new program searched for pixels more than 3.5 σ away from the mean in 25 of our science images. When we find a bad pixel, we set it to the median, then run it through the program again as many times as it takes until we can't detect any more. This process failed for only 2 or 3 "hot" pixels, whose locations we noted and added to the bad pixel mask by hand. We eventually apply the bad pixel mask at the beginning of our mosaic program and use it again later on to construct the exposure map. Without a robust bad pixel detection program and complete 256 x 256 bad pixel mask, one can not guarantee reliable photometry.

4. Making a Mosaic

After calibrating our data, we then combine the images into a single larger image called a mosaic. The big picture goal of making a mosaic is to construct an image with more effective exposure time than any single image could ever have. Individual images will saturate in about 20 seconds based on the sky alone and images with bright stars saturate after a few seconds. Thus it becomes impractical to take a single, long exposure image as all useful information will be quickly washed out. With a mosaic, we get around this saturation limit by taking many short exposure images and combining them. In our case, we used 49 images each with 10s exposures for a maximum effective exposure time of 490s or ≈ 8.2 minutes. Longer effective exposure times give you a higher signal to noise ratio and allow you to detect faint stars and other features that could never be detected in individual images. Indeed, with the mosaic technique, we were able to detect stars as faint as $m \approx 13$ in K and H, and $m \approx 14$ in J. This is remarkable when compared to the previous lab where we struggled to detect 9 and 10th magnitude stars in the K band. The transformation is best illustrated when comparing a single calibrated image to the final mosaic where a huge number of features can now be seen that were virtually nonexistent in the individual image.

Beginning with our original, calibrated 256×256 images, we registered them inside large 512 x 512 superarrays by finding the centroid of a star common to all images and shifting the original 256×256 image inside the superarray in order to place place that star in the center of the super array. We then create an exposure map, which is a 512 x 512 array where each pixel has a value corresponding to the total effective exposure time seen by that pixel. We then stack the registered images, add them up, and divide by exposure map, creating a final mosaic. We did this for our cluster, control field, and standard stars in each band.

4.1. Registering the Images: Finding the Centroid

The use of a weighted mean to find the centroid of a star inside a search box gave us trouble in the previous lab, so we decided to apply the mathematical technique of convolution this time to help us find the centroid of the star we used to register our images.[5] The convolution technique will pick out the brightest pixel in a search box defined around your star, and assuming that the star has a roughly Gaussian profile, then this pixel is our centroid. We repeat this process for all images in the raster pattern and use these centroids to shift the images inside superarrays. The diagram on the following page indicates how we begin with our calibrated 256 x 256 image in the lower left corner of our superarray, and calculate how much to shift it in the x and y directions once we've found the centroid of our aligning star, which now moves to the center of our superarray. I created the diagram using Adobe Photoshop.[6]

---

[5]The mathematics of convolution will be discussed in more detail in the photometry section.

[6]There is a typo that is too late to correct. Where it says "alligning", it should read, "aligning". I also should have indicated more clearly on the diagram that the black dot is the star, but I think people will figure it out.

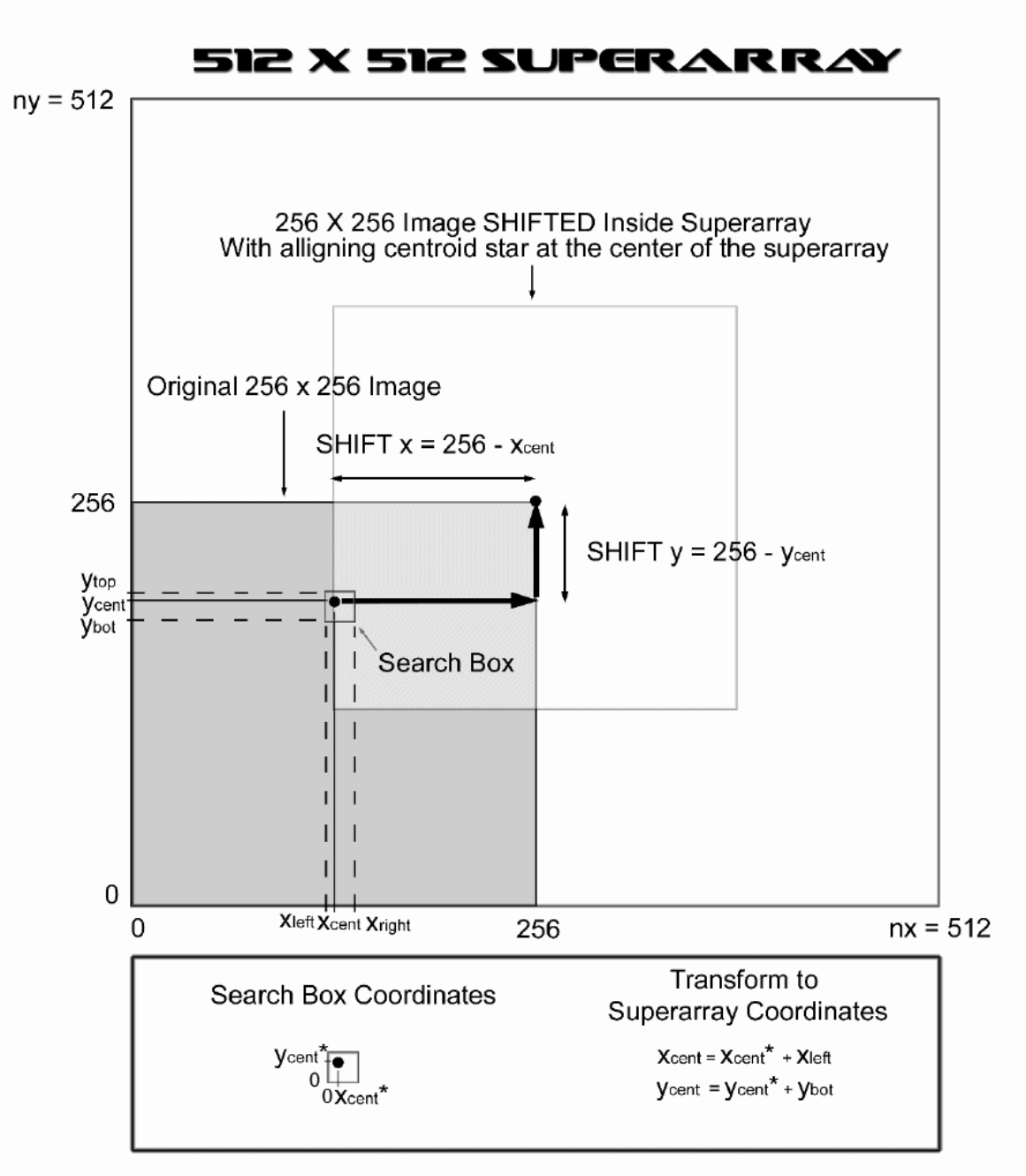

Fig. 2.— We define a search box around our star (black dot) with edge coordinates $[x_{left}, x_{right}], [y_{bot}, y_{top}]$. Given the star's centroid coordinates inside our search box, x^*_{cent} and y^*_{cent}, we find the centroid coordinates inside our superarray by the formulae: $x_{cent} = x^*_{cent} + x_{left}$ and $y_{cent} = y^*_{cent} + y_{bot}$. Given the star's superarray coordinates (x_{cent}, y_{cent}), we now shift the star to the position $(nx/2, ny/2)$ at the center of the superarray by the following: SHIFT by $|nx/2 - x_{cent}|$ in the x-direction and SHIFT by $|ny/2 - y_{cent}|$ in the y-direction. In a case where your superarray has $nx \geq 512$ and $ny \geq 512$, this technique will always work for an original 256 x 256 image.

There are no obvious problems with making your superarray arbitrarily large. However, there are subtle problems with making it too small. Certainly, it must be bigger than your original 256 x 256 array, but how much bigger? The quantitative answer is that it must be at least 2 times as big. For example, we used a 512 x 512 superarray, which was exactly twice the size. Starting with your original 256 x 256 image in the lower left corner, if you want to shift it so your aligning star is in the center of the superarray, you can run into difficulties if your superarray is too small. If the required shift is up and to the right, then there's no problem, but if the required shift has any component down or to the left, then the images go crazy. This is because arrays in IDL have the topology of a 2D torus or donut, in the sense that images shifted off the edge inside a superarray will wrap around to the opposite side. In any case, this wrap around effect must be avoided when producing mosaic images. As it is, the only way to ensure there will be no wrap around effects here is to guarantee that all shifts will necessarily be up and to the right. The best way to do this is to make the superarray more than 2 times as big as the original array. In the extreme case where the original image begins in the lower left hand corner of a 512 x 512 superarray and the aligning star is in the upper right corner of that original 256 x 256 image, then no shift is required since the aligning star is already at the center of the superarray at coordinates (x,y) = (256,256). All other nontrivial SHIFTS will necessarily be up and to the right. Once we register all the images, we can add them up in a superstack and divide by the exposure map to create our final mosaic.

4.2. Creating an Exposure Map

After aligning the images, we wish to create an exposure map, which is a superarray where each pixel on the "sky" has a value corresponding to the effective exposure time (in seconds) that it received as the raster pattern was swept out. For example, if a pixel was near the center of the raster pattern and thus near the center of the cluster, it might have been imaged in all 49 of the 10s exposures, and would thus have an effective exposure time of 490s in the exposure map. If that piece of the cluster happened to fall on a bad pixel in one of the images, then it would lose that 10s exposure and get a value of 480 in the exposure map. If it was never imaged at all, then its value will be 0. Thus the pixel values in our exposure map range from 0 to 490, in increments of 10, with units of seconds. To create the exposure map, we register the bad pixel mask in the same pattern that we used to register the original calibrated science images, creating a super bad pixel mask. We then multiply this by the exposure time per image of 10s. If individual images had different exposure times, the process would be somewhat more complicated.

It should be noted that we do not multiply the super bad pixel mask by the superstack of aligned science images to correct for bad pixels in the flattened superarray. This will artificially inflate your pixel values by factors of 1 to 49. Bad pixel correction is accomplished at the beginning of the centroid process by applying the 256 x 256 bad pixel mask to each of your individual calibrated 256 x 256 science images. The only purpose of registering the bad pixel mask is to create the exposure map. We ran into problems with this and had to redo our entire set of photometry data. This should be made more clear to students earlier in the process.

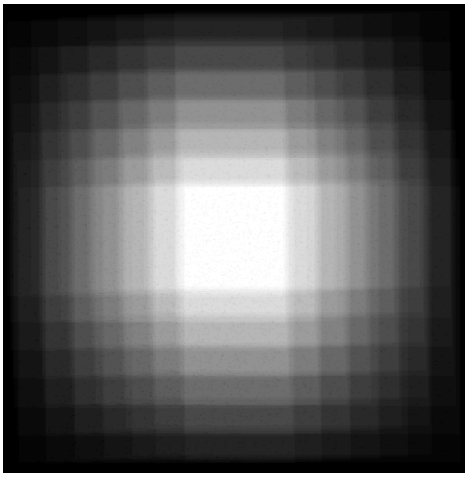

Fig. 3.— An image of the 512 x 512 exposure map. Pixel values range from 490 (white) to 0 (black) in increments of 10. The units of the image are in seconds/pixel. The white pixels ended up being at the center of the cluster and were imaged most, up to 490s $\approx$ 8.2 minutes. The black ones were never imaged. The "crystal" structure is a reflection of the layered overlap given by the geometry of the raster pattern in space. The apparent skewness and blurred tiers of the exposure map is a result of the imperfect pointing of the telescope as we instructed it to complete the raster pattern.

4.3. Making the Final Mosaic

To create the final mosaic, we created a superstack of the aligned superarray science images, and divided by exposure map. This puts the final mosaic in units of counts per second in each pixel. Even so, it is easy to see that the total counts were greatest near the center of the image where the signal to noise ratio was highest and more features can be discerned. Near the edges, few or no stars were imaged. Indeed, the exposure map has many pixels with a value of zero. To avoid dividing by zero when we divide by the exposure map, we set these values to an arbitrary negative number. (we chose 10^{-10}). However, we could have set it to any nonzero number because the corresponding pixels in the superstack were already set to zero by default in the creation of the superarray. The choice of negative number would have been useful if we had needed to flag those pixels later. As it was, we didn't need to reset them to zero, and the final mosaic worked out fine. See the example on the next page of a combined greyscale mosaic of NGC 1333 for all 3 bands.

To emphasize the cool features in the image, I wrote a quick program which creates tricolor images by combining the mosaics from the K, H, and J bands. In order of decreasing wavelength, K, H, and J get assigned the colors R, G, and B, which when combined form a false color image that is nevertheless qualitatively accurate in regard to which photons have the highest (J) and lowest (K) energies. And they look awesome, as evidenced by the color images I included on the next page of this report, which I put them all together in Photoshop both to save paper.

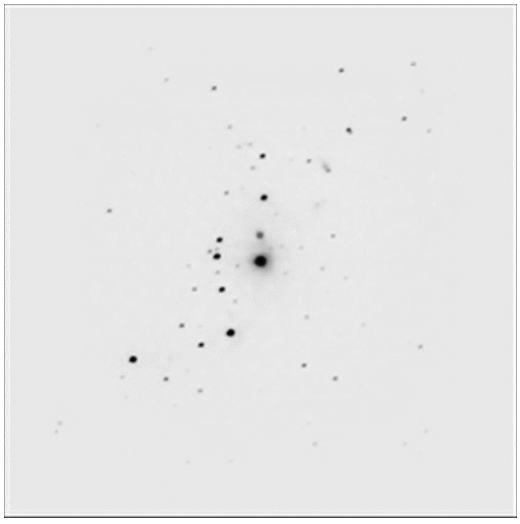

Fig. 4.— Greyscale mosaic of NGC 1333 combining the K, H, and J bands. Regions near the center had greater effective exposure time (49 images x 10 sec exposures x 3 bands $\approx$ 25 minutes!) than regions near the edges, as seen by the number of features that can be discerned towards the center. More detail can be seen in the tricolor images, as shown on the previous page.

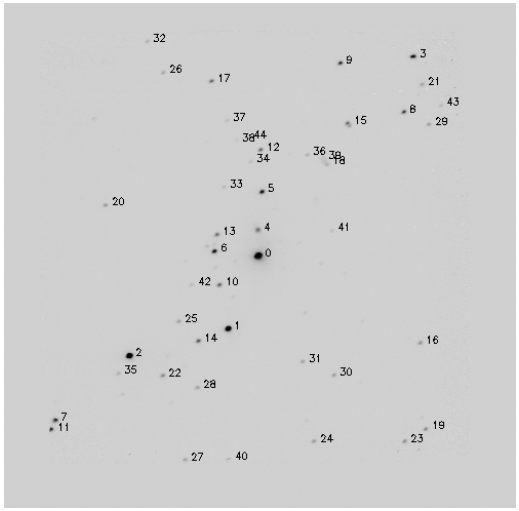

Fig. 5.— Greyscale mosaic of NGC 1333 combining the K, H, and J bands, with the stars numbered in order of increasing brightness from 0 to 44. We only labeled stars that could be seen in images in all 3 bands, ending up with a total of 45. These are the stars we performed photometry on, as described in the next section. This picture will be worth referring to when viewing the tables of photometry data, which list the magnitudes in each band for each star number.

5. Photometry - Science From Pretty Pictures

Once we have a mosaic, we can perform photometry to find the apparent brightness of the stars in our cluster and control field in all 3 bands. We also observed infrared standard stars during our observation run, enabling us to perform differential photometry. We performed photometry on our mosaic image using the technique of convolution as an automated alternative to the type of manual aperture photometry we used in the previous lab. In the end, we chose only to perform photometry on stars which appeared in all bands. This turned out to be 45 for our cluster and 14 for our control field. This created a bias, which cut off the dimmest stars in our image, but we wanted to be able to compare stars with apparent magnitudes in all bands. We detected stars as bright as $m \approx 5$ in all bands after correcting for extinction, which will be discussed in the next section. But thanks to the large effective exposure time and high signal to noise ratio of the mosaic, we were also able to detect stars as dim as $m \approx 13$ in K and H, and $m \approx 14$ in J. The central part of the mosaic had a very high signal to noise ratio (SNR ≈ 100), while it was much lower toward the edges (SNR ≈ 5). As far as extinction goes, the camera sees the reddened magnitudes, but the magnitudes we quote here are the true apparent magnitudes of the star that are corrected for reddening. Nevertheless, when we are talking about what the telescope can detect, we are talking about values that suffer from reddening. In any case, any corrections for reddening give the stars brighter magnitudes, and the magnitude limit of our survey only sees photons, it doesn't care if they are reddened or not. Since we only observed stars with SNR ≥ 5, in principle we could detect stars at SNR $= 1$. This means that our magnitude limit is probably fainter than $m \approx 14$ in each band, probably closer to $m \approx 15$ or 16, with the faintest stars most easily detectable in the J band.

5.1. Review of Differential Photometry

To briefly review differential photometry, if we want to measure the magnitude m of our star, we must measure the number of counts N we receive from it during an exposure time t, and measure the same quantities N_s and t_s for a star of known magnitude m_s under identical observational conditions. We can then calculate m in a given band from the equation:

$$m = -2.5\ log_{10}\left(\frac{Nt_s}{tN_s}\right) + m_s \tag{8}$$

An alternative to measuring N and N_s in all bands is to measure the $K - value$ for our camera in all band. To review the previous lab, the $K - value$ is a constant for any band, has units of $counts/s$ and is given by:

$$K = \frac{N}{t}\ 10^{0.4m} = \frac{N_s}{t_s}\ 10^{0.4m_s} \ => m = -2.5\ log\left(\frac{N}{Kt}\right) \tag{9}$$

Notice that the above equations follow from one another. In particular, we chose the second method and measured K from our standard stars in the field SAO56596. The results are summarized in the plot on the following page.

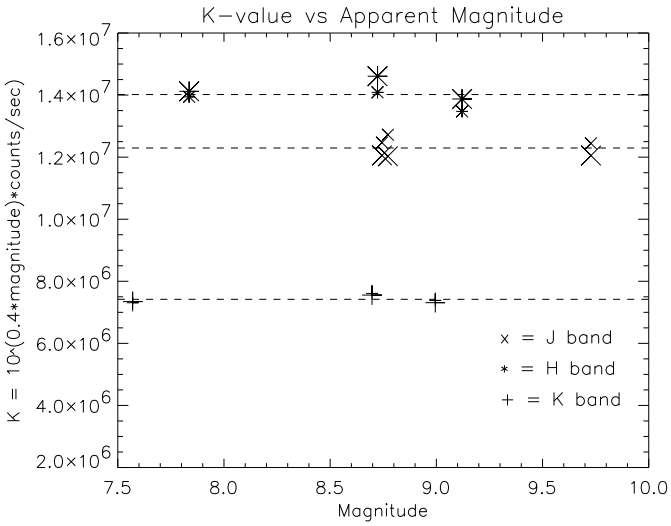

Fig. 6.— We observed 3 standard stars each in the K, H, and J bands all with 2 and 4 second exposures. The smaller plot symbols for each band are for the 2 second exposures, and the larger ones are for the 4 second exposures. We then measured the conversion factor or $K - value$ for each band. As the above plot shows, for a given band, the best fit $K - value$ is a constant, independent of both the star's magnitude and exposure time, as expected. Errors from the standard deviation of the mean of the values for each band are less than 3%, (1.76% in K, 2.64% in H and 2.36% in J). Error bars are thus left off the plot for clarity.

5.2. CONVOLUTION: An alternative to aperture photometry

Instead of constructing an aperture and sky annulus manually for each image, in this lab, we used the mathematical technique of convolution to perform photometry automatically on an arbitrary number of the brightest stars in our mosaic images for each band. Convolution actually does aperture photometry on every pixel in your image, and this allows you to pick out the pixel centered inside the aperture with the highest number of counts. This number of counts is then the photometry value for that star. We first find the brightest pixel in the image, calling its convolution value the number of counts for the first star. Then we mask that star out so its other bright pixels will not be mistaken for stars. We then find the photometry for the second brightest star and so on. This technique assumes that the profile for a typical star is roughly Gaussian.

Regarding the mathematics of Convolution, if you have a continuous *Stimulus* $S(x')$ such as your star field and a continuous *Response* $\phi(x)$ such as your detector's Point Spread Function, your continuous Convolved Image $C(x)$ is given by:

$$C(x) = \int_{x'=-\infty}^{x'=\infty} S(x')\phi(x - x')dx', \tag{10}$$

For discrete 2D images such as the ones we are dealing with, the discrete convolved image $C(x, y)$ can be extracted from the 2D Convolution Theorem:

$$C(x, y) = \int\int dxdy(\Sigma\ A_i\delta(x - x_i)\delta(y - y_i)\phi(x - x_i, y - y_i)) \tag{11}$$

Where the quantity $\delta(x - x_i)$ reflects how much your instrument's point spread function shifts the true pixel where the star would appear for a perfect detector response. The above expression is often written in shorthand as $C = S * \phi$, where $*$ is the convolution operator and represents performing the double integral and sum over the product of the stimulus $S(x, y) = A_i\delta(x - x_i)\delta(y - y_i)$, and response $\phi = \phi(x - x_i, y - y_i)$, where A_i is the star brightness. $C(x, y)$ is a final convolved image where each pixel now has a value that is the result of the convolution performed at that pixel with coordinates (x_i, y_i).

5.3. Making a Kernel: Top Hat and Moat

In IDL, instead of using the stimulus-response Behaviorist jargon, we talk about convolving our image with a kernel. Here the kernel is our response. In our case, we want to pick a kernel whose convolution with our image will simulate the process of aperture photometry. The idea is to pick a kernel with a positive height top hat and a negative height moat, such that the volumes of the top hat and moat are equal. Making the moat negative with the same volume as the top hat is effectively the same thing as finding the median sky brightness in your annulus, and subtracting that value for every pixel in your aperture. We then Convolve our image with this kernel, and this effectively performs aperture photometry for as many stars as we wish in our image.

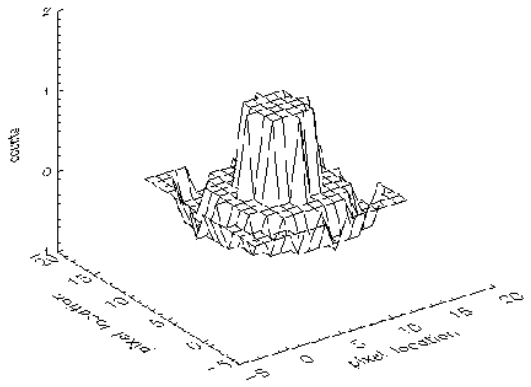

Fig. 7.— Our kernel with top hat and moat. The dimensions are {top hat radius: 3 pixels, moat inner radius: 6 pixels, moat outer radius: 8 pixels, top hat height: 1 count, moat depth: - 0.353659 counts} These dimensions are constructed to make the volumes of the top hat and moat equal.

5.4. Photometric Errors

Propagation of errors led us to believe that photometric errors due to flat fielding, dark subtraction, and sky subtraction were all less than 0.1% and were thus negligible compared to the errors from Poisson statistics and from calculating the $K - value$. Fully propagated photometric errors ranged from $\approx 2\%$ for the brightest star which had the highest signal to noise ratio of $SNR \approx 100$, and as high as $\approx 20\%$ for the stars with the lowest $SNR \approx 5$. Overall errors for all stars in each band are roughly 9%in K, 10% in H, and 15% in J. Below we list our best photometry values, which are the apparent magnitudes of the stars we performed photometry on in all 3 bands. One column lists the observed values that have not been corrected for reddening, the other lists red-corrected values for the M.S. we were able to find the reddening for. Calculating the reddening is discussed in the next section. Errors are not included in the table.

Star #	K	J	H		K_o	J_o	H_o
0	7.2	9.3	8.0		5.8	5.7	5.8
1	8.3	9.9	8.9				
2	8.4	8.9	8.6		7.9	7.8	7.9
3	9.2	11.3	10.2				
4	9.6	11.5	10.3		8.2	8.0	8.1
5	9.6	11.3	10.3				
6	9.7	11.6	10.5				
7	9.9	12.4	10.9				
8	10.0	11.8	10.7		8.8	8.8	8.8
9	10.1	12.8	11.2				
10	10.2	11.2	10.5		9.6	9.6	9.6
11	10.2	12.6	11.3				
12	10.3	12.9	11.3		8.5	8.5	8.5
13	10.5	11.5	10.8		9.8	9.9	9.8
14	10.5	11.9	10.9		9.8	10.2	9.9
15	10.5	14.4	12.2				
16	10.6	12.0	11.2		9.6	9.4	9.6

Table 3: Magnitudes for the 45 stars measured in NGC 1333 that could be detected in the images for all 3 filters. The first three columns K, J, and H represent magnitudes that have not been corrected for reddening. The last three columns K_o, J_o, and H_o list the reddening-corrected magnitudes for M.S. stars only. We could not calculate reddening values for stars not on the M.S., as discussed in the next section. For example, the red corrected apparent K magnitude is given by $K_o = K - A_k$, where A_k is the amount of reddening in the K band, in magnitudes. Table Continued on next pg...

Star #	K	J	H		K_o	J_o	H_o
17	10.7	14.8	12.8				
18	10.9	12.7	11.6				
19	11.0	13.6	12.0		9.2	8.9	9.1
20	11.0	14.1	12.4				
21	11.1	12.0	11.4		10.5	10.6	10.6
22	11.2	12.2	11.6		10.4	10.4	10.4
23	11.2	12.7	11.9				
24	11.3	13.3	12.0		9.8	9.6	9.8
25	11.3	14.5	12.3		9.7	10.4	9.8
26	11.4	12.9	12.0		10.3	10.1	10.3
27	11.4	12.8	11.9		10.8	11.2	10.8
28	11.5	12.8	11.9		10.9	11.4	11.0
29	11.5	12.5	11.9		10.7	10.5	10.7
30	11.5	12.5	11.9				
31	11.7	14.3	12.7		9.8	9.6	9.8
32	11.8	14.2	13.1				
33	11.9	13.3	12.4		10.8	10.6	10.8
34	11.9	13.5	12.4		11.0	11.3	11.1
35	12.1	14.1	12.7		11.1	11.6	11.2
36	12.2	14.7	13.1		10.3	10.0	10.2
37	12.2	13.4	12.7				
38	12.3	13.5	12.8				
39	12.4	14.5	13.4				
40	12.6	14.6	13.1				
41	12.6	14.5	13.5				
42	12.6	14.2	13.1		11.9	12.3	11.9
43	13.0	14.9	13.9				
44	13.2	14.6	13.7		12.2	12.2	12.2
45	13.3	14.9	14.0				

Table 4: Continued ... Magnitudes for the 45 stars measured in NGC 1333 that could be found in the images for all 3 filters. The first three columns K, J, and H represent magnitudes that have not been corrected for reddening. The last three columns K_o, J_o, and H_o list the reddening-corrected magnitudes for M.S. stars only. We could not calculate reddening values for stars not on the M.S. For example the red corrected apparent K magnitude is given by $K_o = K - A_k$, where A_k is the amount of reddening in the K band in magnitudes.

6. Using a Color-Color Diagram: Correcting for Reddening

Extinction by dust makes stars appear dimmer and redder, as typical dust grains absorb light while preferentially scattering blue light more than red light, which can reach our telescope. The dust contributing to the extinction of our cluster comes from both the dust along the line of sight in the space between us and the cluster and the dust intrinsic to the cluster, which we expect there to be a lot of for a star forming region. For our control field, since we know it is not a cluster that is intrinsically rich in dust, we can reasonably say that the extinction there is caused by intervening dust and not dust in the control field itself. To determine the amount of reddening due to extinction for our cluster and control field, we construct a $(J-H)$ vs $(H-K)$ color-color diagram which is useful because it is independent of the distance modulus to the cluster and the control field.

It should be noted that while our cluster consists of objects at roughly the same distance, the control field consists of many objects at varying distances. Interstellar extinction only allows us to see out to a certain distance before stars become too dim. Thus we can see only the stars in the control field that are close enough to not be entirely obscured by dust. But since we do not know the relative distances of the cluster and control field, we can not assume anything about the relative amounts of intervening dust between us and the both sets of objects.

Reddening is typically measured in visual magnitudes, A_V, where we can relate a star's reddening A to reddening in the near-infrared bands from Table 1 (as shown earlier), which lists A/A_V values based only on the intrinsic physics of dust grains. To summarize Table 1, $A_V = 1.000A_V$, $A_K = 0.112A_V$, $A_H = 0.175A_V$, and $A_J = 0.282A_V$.

6.1. Deriving the Reddening Vector: Finding Reddening Values for Stars in the M.S. Band

If we know what the unreddend color of a star should be, we can calculate how much it has been reddened and correct for it. For M.S. stars, we know the relevant $(J-H)$ and $(H-K)$ colors as found in Table 4 in the lab. Thus we can plot the locus of M.S. stars and see how far each of our stars lies away from this locus in the color-color diagram. The geometric distance D from the M.S. locus will be proportional to the reddening A_V in magnitudes. To calculate the reddening A_V, we first construct the $(H-K)-(J-H)$ reddening vector $\vec{A}$, whose slope and direction is the same for all stars (it is based only on the physics of dust grains) but whose magnitude $|\vec{A}| = D$ will vary from star to star depending on how much dust is obscuring it. From the table listing A/A_V values, it follows that the $(H-K)-(J-H)$ reddening vector $\vec{A}$ is given by:

$$\vec{A} = (A_H - A_K,\ A_J - A_H) = (0.175A_V - 0.112A_V,\ 0.282A_V - 0.175A_V) = A_V(0.063,\ 0.107) \quad (12)$$

The slope of this vector will always be $\frac{0.107}{0.063} = 1.7$. The geometric length of the vector is:

$$D = |\vec{A}| = A_V\sqrt{(0.063)^2 + (0.107)^2} = 0.124A_V \ \Rightarrow A_V = 8.05D \quad (13)$$

where the conversion factor between geometric length and reddening in visual mag is 8.05 mag.

From the color-color diagram below, we measure the geometric distance D using the relation:

$$D = \sqrt{(\Delta(H-K))^2 + (\Delta(J-H))^2} \tag{14}$$

where $\Delta(H-K)$, for example, denotes the color excess in $(H-K)$, which is the shift in $(H-K)$ color that we measure for a star relative to where it should have appeared on the UN-reddened Main Sequence. After measuring D, we use the relation $A_V = 8.05D$ to calculate the reddening in magnitudes for each M.S. star. We can not calculate reddening values for non M.S. stars here, since we don't know the locus of their colors. In the end, we calculated average reddening values of $A_V \approx 9.5$ mag toward our cluster and $A_V \approx 1.7$ mag toward our control field. The results are discussed more explicitly in the captions of the following color-color diagrams.

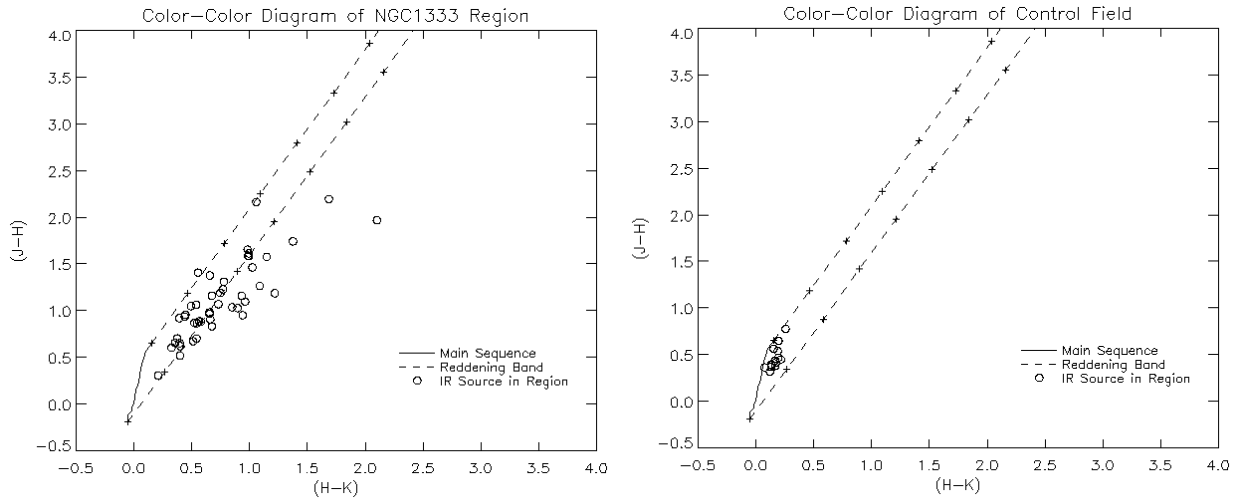

Fig. 8.— Here we display the color-color diagrams four our cluster and our control field. The circles represent the $(J-H)$ and $(H-K)$ colors for infrared sources in the images. The two dashed lines represent our Main Sequence Reddening Band, where the. tick marks occur every 5 visual magnitudes. The lines forming the M.S. band have the same slope as the reddening vector $\vec{A}$ (slope = 1.7) and they are extrapolations from the lower and upper mass ends of the M.S. We can only calculate reddening for stars that can be extrapolated back to the M.S locus along a line with the slope of the reddening vector, i.e those in the M.S. Band. Stars outside this band are either PMS stars or giants, and since we do not know the locus of their colors, we can not calculate their reddening values. For our cluster, nearly half of the stars were not on the M.S., in contrast with our control field, where all stars lie on the M.S. In calculating D and A_V, We made the reasonable approximation that the M.S. locus could be fit as a straight line. This is not actually the case, but the approximation is likely to admit only small errors. Overall we measured an average reddening of $A_V \approx 9.5$ toward our cluster and $A_V \approx 1.7$ mag toward our control field. The relatively small extinction towards our control field relative to our cluster is another strong indication that the control field is not a star cluster.

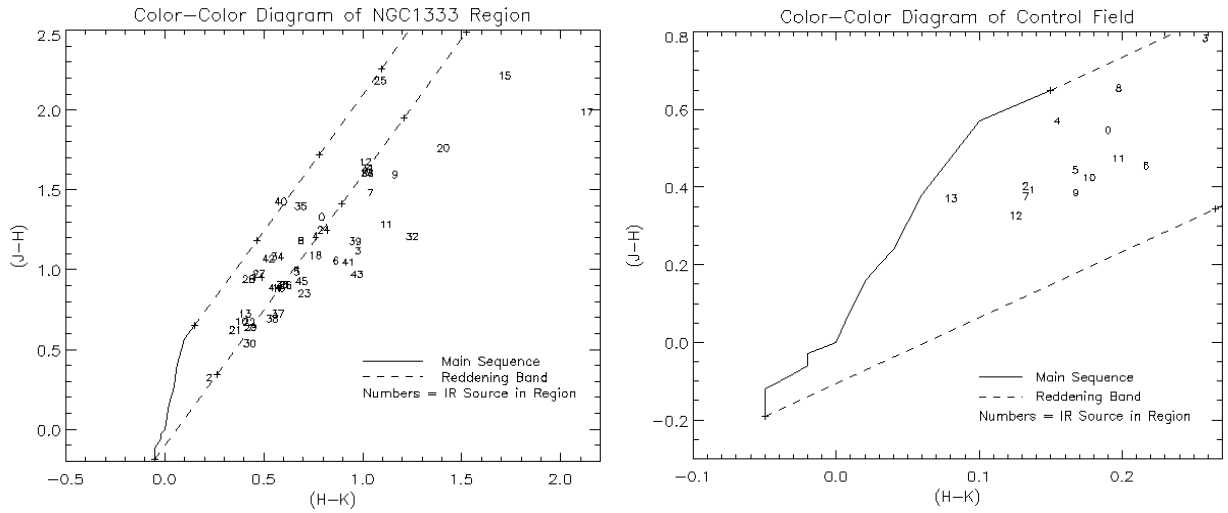

Fig. 9.— Here we plot the color color diagram for our cluster and control field with stars numbered in order of increasing brightness, ranging from 0 to 44 in the cluster field and 0 to 13 in the control field. We also zoom in on the portion of the diagram with stars to make the numbers more readable. Again tick marks occur on the M.S. band every 5 visual magnitudes, and the average reddening was $A_V \approx 9.5$ for the cluster and $A_V \approx 1.7$ mag for the control field. Tables of the photometry data for the control field are displayed on the next page.

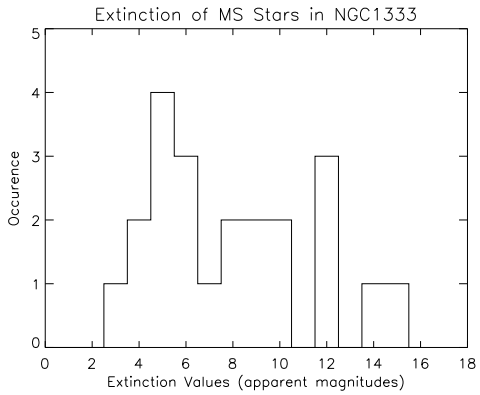

Fig. 10.— Here we plot a Histogram of A_V Reddening Values in our cluster in an attempt to test whether our dust model is reliable. The fact that it roughly follows a Gaussian distribution allows us to calculate the errors using Poisson statistics. Using the Standard Deviation of the Mean of these values as the error, we calculate an error in A_V for each star of $\delta A_V \approx 0.8$ mag. If the distribution had been systematically different, such as cutting off all stars in a given magnitude range, our model would need to be modified.

Here we display a table of the photometry data for the control field, where reddening values could be found for all stars in the field since they were all M.S. stars. We actually had 2 more stars whose data did not make it onto the table.

Star #	K	J	H		K_o	J_o	H_o
0	9.2	9.9	9.4		9.0	9.1	9.5
1	11.1	11.7	11.3		11.0	11.1	11.3
2	11.4	12.0	11.6		11.3	11.4	11.7
3	11.5	12.5	11.7		11.3	11.4	11.9
4	11.5	12.2	11.7		11.4	11.6	12.1
5	11.7	12.3	11.8		11.5	11.5	11.8
6	12.0	12.7	12.2		11.7	11.7	11.8
7	12.0	12.5	12.1		11.9	11.9	12.2
8	12.1	13.0	12.3		12.0	12.1	12.6
9	12.2	12.7	12.3		11.9	12.0	12.1
10	12.2	12.8	12.4		11.9	12.0	12.2
11	12.4	13.1	12.6		12.1	12.2	12.4

Table 5: Magnitudes for the brightest 12 stars measured in our control field that were detected in the images for all 3 filters. The first three columns K, J, and H represent magnitudes that have not been corrected for reddening. The last three columns K_o, J_o, and H_o list the reddening-corrected magnitudes. All stars in the control field fell on the Main Sequence, which which allowed us to correct for reddening, and is what we would expect statistically for a random collection of stars.

7. Luminosity Function

Next we plot the luminosity function for our cluster and our control field in each of the 3 bands. The luminosity function does not really deal directly with luminosity, it is simply a histogram of measured apparent magnitudes binned up to give the most information. The values we plot have been corrected for reddening. The most useful thing a red-corrected luminosity function can tell us is if there are a statistically significant number of stars in our cluster relative to the control field. We definitely do see a larger number of brighter stars in our cluster, further showing it is indeed a cluster while the control field is not. In addition, it tells us the range of apparent magnitudes for stars in our cluster which roughly go from mag 5 to 14 in all bands. It should be noted though, that we created a bias by only performing photometry on the brightest 45 cluster stars and 14 control field stars that could each be seen in all filters. This arbitrarily cut off fainter stars from the luminosity function in various bands. Furthermore, we can not guarantee that individual stars we plot in the luminosity function are actually in our cluster and are not background or foreground stars. This is a very difficult thing to check, but the bottom line is that a given object in the

field of view of NGC 1333 is more likely to be a member of the cluster than not. Thus we can assume most stars in the luminosity function are in the cluster. This does not greatly reduce the statistical significance of comparing the number of stars in the cluster and control field luminosity functions. Alternatively, we could have plotted the luminosity functions that had not been corrected for reddening. Lee Huss did this in his report, so I will reference his work here rather than repeat it. In any case, the luminosity functions below are red-corrected with average photometric errors in all bands of roughly 12%.

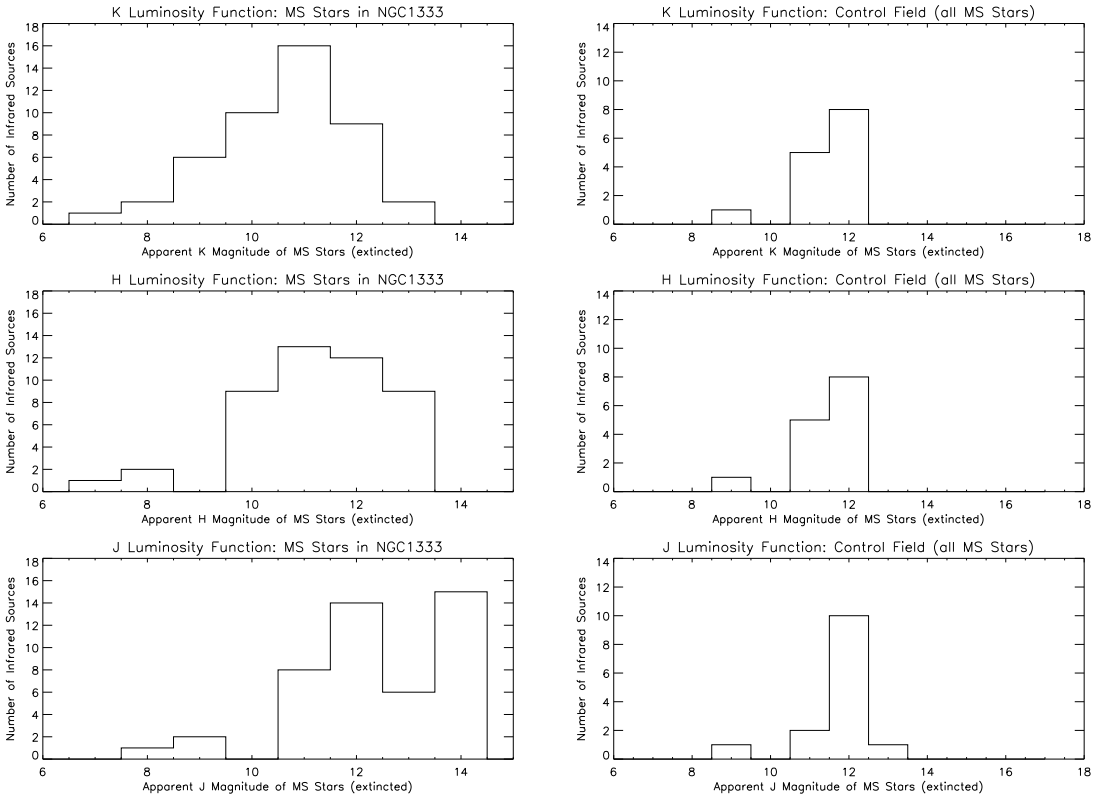

Fig. 11.— Here we show the reddening corrected Luminosity Functions for our cluster and control field in all 3 bands. Despite the fact that we arbitrarily cut off some of the faintest stars by performing photometry only 45 stars, and despite the fact that we can not guarantee that an object in the cluster luminosity function is actually in the cluster, the bottom line is that there are a statistically significant number of stars in the cluster luminosity function compared to the control field luminosity function. This is easily seen by comparing the areas under the histograms, which naturally ends up as the number of objects plotted, 45 for the cluster and 14 for the control field. Assuming the density of random stellar objects is comparable in all directions, one can estimate the true cluster membership by subtracting the luminosity functions and, which in this case, would yield roughly 30 stars in the cluster. But again, this number is not very meaningful as we cut off the faintest stars, most of which probably are cluster members that are faint due to extinction.

8. Using a Color-Magnitude Diagram: Extracting the Age of the Cluster

Another useful way to display our data is to construct a M_K vs. $(J-K)$ color-magnitude diagram for our cluster. As in the color-color diagram, we also can find the red corrected $(J-K)_o$ colors and absolute K magnitudes M_K for the M.S and overplot the locus of M.S. stars. From Table 4 in our lab, we can find $(J-K)_o$ from the relation:

$$(J-K)_o = (J-H)_o + (H-K)_o \tag{15}$$

where the latter reddening corrected colors $(J-H)_o$ and $(H-K)_o$ are known for M.S. stars. Knowing M_V for M.S. stars, we find M_K from the formula:

$$M_K = M_V - (V-K)_o = M_V - \{(V-J)_o - (J-H)_o - (H-K)_o\} \tag{16}$$

where the o subscripts denote values that have all been red corrected. For our actual data, we measured apparent K and J magnitudes for our stars and can use them to find M_K and $(J-K)$. For $(J-K)$, we simply plug in our measured values of $K = m_K$ and $J = m_J$. (Capitol letters are shorthand for apparent magnitudes in that band.) But since we didn't actually measure M_K directly, we need to find it using the known distance modulus to the cluster. Using the fact that the distance modulus is the same for all bands, we see that for the K band in particular

$$K - M_K = (m_K - M_K) = (m-M) = 5\ log\ \left(\frac{D}{10pc}\right) \tag{17}$$

This gives us the simple relation

$$M_K = K - (m-M) \tag{18}$$

Lada et al. (1996) quote a distance to NGC 1333 of $D = 320$ pc, which gives a distance modulus of $(m-M) = 5\ log\ \left(\frac{320pc}{10pc}\right) = 7.53$. This assumed to be a constant for all stars in the cluster because distances between stars in the cluster are negligible compared to their distances from us. With this information, we can now use $M_K = K - (m-M) = K - 7.53$, to find M_K.

As we can see, both axes depend on our observed apparent magnitudes. However, for our data, some of these apparent magnitudes have been corrected for reddening and some have not. In fact, we can only calculate reddening values for stars on the M.S. So when we display our color-magnitude diagram, there will be a remaining population of non M.S. stars that have not been corrected for reddening, which we can specify with different plot symbols. Having specified the locus of M.S. stars, we can look up their corresponding spectral type from Table 4 in the lab and use them to estimate the age of the cluster, knowing which stars we measured are on the M.S. This is discussed in the next section. Calculating how errors in the measurements of both axes combine to effect the final data point is rather tricky. Thus we will make the simple assumption that stars we are interested in lie in a given range of spectral types which encompasses the error region.

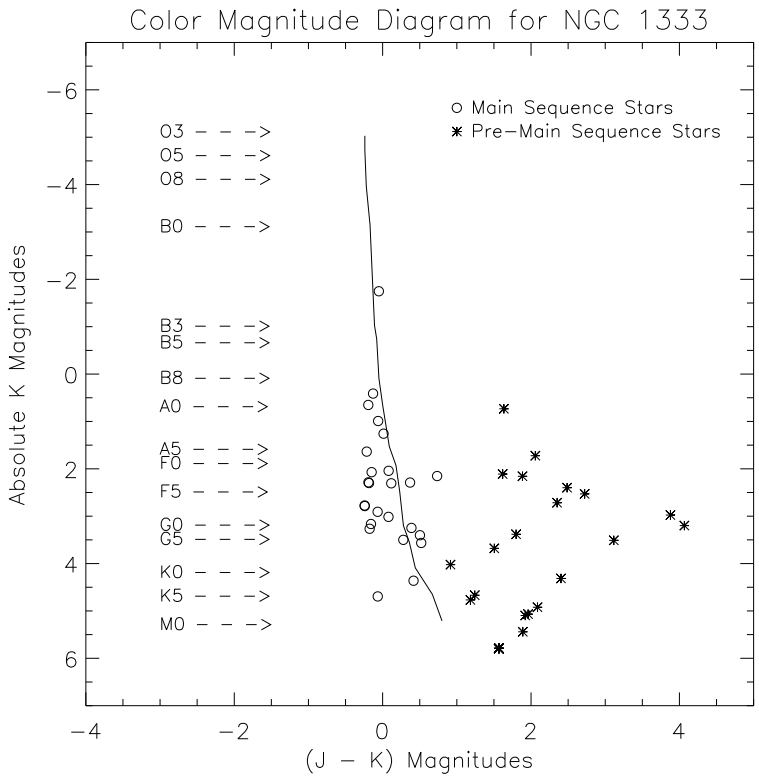

Fig. 12.— The locus of M.S. points have been corrected for reddening, and the corresponding spectral types for the various main sequence stars are indicated with arrows to the left of the M.S. locus. The circles represent M.S. stars in our cluster, and the asterisks denote non-M.S. stars. The most massive M.S. star in the diagram (which is also the brightest star in our image) is probably a $B2$ star ($M \approx 12.36 M_{\odot}$), while the least massive is likely a $K5$ star ($M \approx 0.67 M_{\odot}$). The most massive star can be used to deduce an upper limit for the age of the cluster, which we calculate to be $\approx$ 18 million years, as shown in the next section. Error bars are not shown but are taken into account in our calculations as uncertainties in spectral type classification.

From the above diagram, the most massive star still on the M.S. appears to be a $B2$ star, although the error in M_K absolute magnitudes (error $\approx 12\%$) are certain contribute to errors in spectral type classification. But assuming it is a $B2$ star, if we can calculate the M.S. lifetime of that star, we can arrive at an upper limit for the age of the cluster. We mean an upper limit in the sense that the cluster can not be any older than the M.S. lifetime of the most massive star still on the Main Sequence. All other stars of higher mass will have already died and left the M.S. The cluster thus must be older than their M.S. lifetimes. But if a star is still on the M.S., the cluster can not be older than its M.S. lifetime, since if it was, the star would have already left the M.S. Thus our goal is to calculate the M.S. lifetime of a $B2$ star to find upper limit for the age of our cluster. This method of determining cluster ages is called the Main Sequence Cutoff method.

8.1. Lifetimes of Main Sequence Stars

To calculate the lifetime of M.S. stars, we must use the M.S. mass-luminosity relationship.

$$\frac{L}{L_\odot} = \left(\frac{M}{M_\odot}\right)^\alpha \tag{19}$$

where α is parameter in the power law fit that is theoretically somewhere between 3 and 4, and empirically found to be $\alpha \approx 3.5$, where it should be noted that the power law fit is not perfect for all mass and luminosity ranges on the M.S. A summary of the measured values in the fit can be found on pg. 211 of Carroll & Ostlie. We use this empirical data to justify adopting a model with $\alpha \approx 3.5$. It should also be noted, however, that mass, luminosity, and M.S. lifetime determinations are quite sensitive to your choice of α, often up to more than a factor of 2.

To find a star's M.S. lifetime t, we note that it must be proportional to the star's available fuel M and inversely proportional to the rate at which it burns its fuel $\dot{M}$ (i.e. $t \propto \frac{M}{\dot{M}}$). $\dot{M}$ is shown to be proportional to the star's luminosity L using Einstein's mass-energy equivalence relation $E = Mc^2$.

$$L = -\frac{dE}{dt} = -c^2\frac{dM}{dt} = -c^2\dot{M} \;\Rightarrow\; \dot{M} \propto L \tag{20}$$

From this we see that the star's M.S. lifetime $t \propto \frac{M}{\dot{M}} \propto \frac{M}{L}$. Using the mass luminosity relationship, we can now derive the equation for a star's M.S. lifetime in solar units:

$$\frac{t}{t_\odot} = \left(\frac{M/M_\odot}{L/L_\odot}\right) = \left(\frac{M/M_\odot}{(M/M_\odot)^\alpha}\right) \Rightarrow\; t = t_\odot\left(\frac{M}{M_\odot}\right)^{1-\alpha} \tag{21}$$

where $t_\odot \approx 9 \times 10^9$ years. Now we are prepared to calculate the lifetime of a $B2$ star, the most massive star in our cluster still on the M.S.

Since we do not have data for $B2$ stars in Table 4 of the lab, and Carroll & Ostlie do not have a $M/M_\odot$ ratio for $B2$ stars, we have two choices. We can choose an α and calculate M_{B2} from the $L/L_\odot = 5700$ they give, or we can calculate L ourselves knowing M_V and the bolometric correction BC for a $B2$ star. The first method involves much less calculation, so we will present it here an leave the second calculation to the appendix. Using $\alpha = 3.5$, and $L/L_\odot = 5700$, plugging that into the equation $M/M_\odot = (L/L_\odot)^{1-\alpha}$, we arrive at a mass of $M_{B2} \approx 11.8M_\odot$. Plugging this mass into the M.S. lifetime equation, $t = t_\odot\left(\frac{M}{M_\odot}\right)^{1-\alpha}$, we arrive at an age of roughly 19 million years. This then is the upper limit for the age of our cluster. It is not a very tight upper limit, but it is consistent with the cluster lifetime of 1-2 million years estimated by Lada et al. (1996).

The probable $B2$ star in question was the brightest star in the image, and thus had the highest signal to noise ratio (SNR ≈ 100). Thus the error in its m_K apparent magnitude before correcting for reddening is small ($\approx 2\%$ error from all bands). However, its reddening value of $A_V = 1.4$ has a large error $\approx 15\%$, and this contributes enough to the final error in M_K enough to put the spectral classification in doubt. If anything, the star could easily be a younger $B1$ or $B0$ star. Thus we can perform a rough error analysis by calculating upper limit ages of the cluster using these different spectral classes. The results are summarized in the table on the next page.

Spectral Type	$L/L_\odot$	$M/M_\odot$	t (10^6 years)
B0	52000	17.5	7*
B1	16000	15.9*	9*
B2	5700	11.8*	19*
B3	1900	7.6	57*

Table 6: *Using a model with $\alpha = 3.5$, we tabulate information for stars with spectral type close to the probable spectral type of the brightest star in our image ($B2$), from which we are estimating the age of the cluster. The $L/L_\odot$ information and two of the mass ratios were found in Appendix 13 of Carroll & Ostlie. Quantities derived here are marked with an asterisk*.*

Spectral Type	BC	M_V	$L/L_\odot$	$M/M_\odot$	t (10^6 years)
B0	-3.16	-4	62000*	23.4*	3*
B1	-2.7	-3.2	19000*	16.7*	8*
B2	-2.35	-2.4	6700*	12.4*	17*
B3	-1.94	-1.6	2200*	9.0*	37*

Table 7: *Again using a model with $\alpha = 3.5$, we tabulate information relevant to estimating the age of the cluster. This time, instead of taking luminosities from tables, we calculate them from BC (bolometric corrections) and M_V absolute magnitudes. The BC and M_V values are found in Carroll & Ostlie Appendix 13. We calculate all other quantities marked with an asterisk*. As we can see, we get a slightly smaller upper limit for the age of our cluster using this method, 17 vs. 19 million years. In any case, the methods are consistent to within the same order of magnitude. Derivations required to make these calculations can be found in the APPENDIX.*

Thus if our star is actually a $B0$ or $B1$ star as opposed to a $B2$ star, then our cluster is younger and we have a tighter upper limit for its age by roughly a factor of 2. If it was a $B3$ star, the upper limit would be raised by roughly a factor of 3. Determining a lower limit is more difficult, since the absence of high mass stars on the color-magnitude diagram could indicate that they have died and left the M.S. or that they never existed in the cluster in the first place. One can not tell for sure which stars in the cluster have left the M.S. without spectra of the stars in the giant branch. Thus it is more useful for us to quote an upper limit, which says that the cluster can not be older than the M.S. lifetime of the most massive M.S. star in the cluster.

Finally, we estimate the mass of the faintest stars we can detect by using the faintest M.S. star in our diagram (error $\approx 4\%$ from all bands) with a signal to noise ratio of close to 5, near the detection limit of SNR = 1. It appears to be of spectral type $K0$, which has a mass of roughly $0.67 M_\odot$. If anything, the spectral type classification is in error and the star is actually less massive. And certainly there are less massive, fainter stars in the field since we only did photometry on the stars that could be seen in all bands, which necessarily excludes the faintest stars.

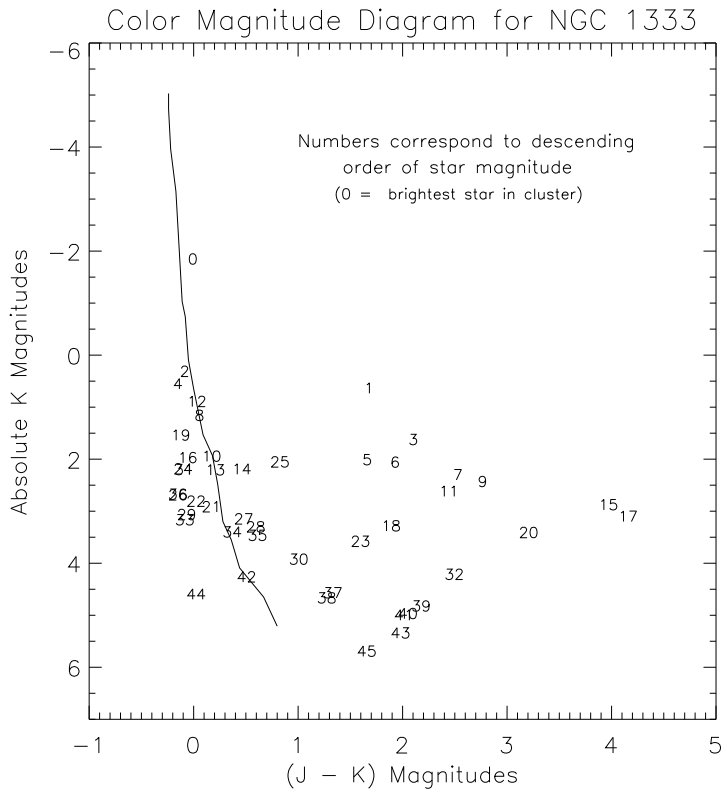

Fig. 13.— Here we show another version of the color-magnitude diagram with stars numbered in order of increasing brightness, from 0 to 44. Star 0 is the brightest star in the image and the one we use to estimate an upper limit for the cluster's lifetime $\approx$ 19 million years. Star 44 is the dimmest star in the image and we use it to estimate the mass of the faintest stars we can detect ($M \approx 0.67 M_{\odot}$). Both stars are on the M.S., and in general, the points scattered closest to the M.S. locus are indeed on the M.S.

9. Conclusion

This report was an excellent synthesis of our previous labs and got us involved with some genuine astronomical observations and theoretical analysis that forced us to act nearly as professional astronomers. It was undoubtedly helpful to analyze a star cluster such as NGC 1333 that had been studied in the literature, most notably by Lada et al. (1996) and Aspin et al. (1994). The idea that a mosaic can increase your effective exposure time indefinitely without worrying about saturation is an extremely useful, really driving home the point that the Hubble deep field wasn't created by simply pointing at a patch of the sky forever, but by combining shorter images. The technique of convolution was quite helpful at making our photometry more tractable. In the end, we determined that our cluster was indeed a cluster, but we did not apply sophisticated techniques

such as the K-S test, which would be kind of like using a laser saw to make a sandwich, in my opinion. Again, I was inspired to include a lot in this lab, mostly because I am writing the report that I would like to have seen at the beginning of the project. In my mind, this involves being extremely detailed. I have been told, in fact, that if I was an IDL routine, you'd have to flag me with the ,/verbose command. I also went a little bit overboard by constructing the image shifting diagram in Photoshop, but what can I say, I'm crazy. And the images were so impressive that I felt compelled to piece them together in Photoshop as well. In the end, I'm impressed by the clear connection between theory and observation, where we can throw around some ideas about the formation and evolution of stars, scribble a few diagrams on the blackboard, and actually get what we expect when we observe these things. As a potential theoretical physicist, I will be the best at my job only if I strive to never forget this remarkable connection.

10. APPENDIX

Rather than trusting the luminosities given in Carroll & Ostlie, we can instead choose to trust the absolute visual magnitudes M_V and Bolometric Corrections BC for M.S. stars and use those to calculate the luminosity, mass, and M.S. lifetime of the relevant M.S. stars. This process yields a smaller number for the age of our cluster. Beginning with the inverse squared law

$$F = \frac{L}{4\pi d^2} \;\; => \;\; L = F 4\pi d^2 \tag{22}$$

we note that to correct for the fact that we are observing in a given band, we must apply the bolometric correction if we hope to find the luminosity of the star over all wavelengths. In other words, we want to determine the total energy per unit time emitted from the star even though we only have observed the star in maybe one or two bands. To convert to bolometric apparent magnitudes, from visual absolute magnitudes we use the relation:

$$m_{bol} = BC + (m - M) + M_V \tag{23}$$

We next note that the total flux in all wavelengths in terms of the integrated flux of Vega will be

$$F = F_{\nu_o} 10^{-0.4 m_{bol}} \tag{24}$$

where $F_{\nu_o} \approx 2.69 \times 10^{-5} \frac{erg}{scm^2}$ is arrived at using the facts that Vega is an $A0$ star with $L/L_\odot = 54$, and is at a distance of 8pc. Noting that $L = F_{\nu_o}\ 10^{-0.4 m_{bol}} 4\pi d^2$ and that our NGC 1333 cluster at a distance of 320pc, we arrive at the equation $L = L(BC, M_V)$ for our cluster.

$$L = 3.229 \times 10^{35}\ 10^{-0.4(BC + M_V)}\ \frac{erg}{s} \tag{25}$$

We can now use this to calculate the luminosities, masses, and lifetimes of the desired M.S. stars using previous methods. A table of the calculated values was presented earlier, with this derivation referenced.

ACKNOWLEDGMENTS

As a four week lab, this report was marginally less stressful to complete in the sense that, while we are still pulling an all nighter to finish the writeup, we are all operation on roughly 30% more sleep over the last 72 hour period, as compared to last time. In this spirit of relative awakeness, I would like to acknowledge the various contributions of myself and my fellow group members in completing this report. Personally, I focused mostly on making our mosaic program (or rather 4 separate programs), which finds centroids using convolve, registers the images, creates an exposure map and generates the final mosaic. I would like to especially thank Lee Huss, who spent a great deal of time chugging through the mosaic jungle with me while we fixed about 90 bugs in the program. In the end the infrastructure of these programs is enormous. It practically has its own zip code. In the end of the mosaic era, I also worked on a program that generates tricolor images to make our mosaics look that much cooler. Lee and I also spent time constructing the color-color diagram, correcting for reddening, and making the luminosity functions. Finally, I spent a lot of time deriving the lifetimes of Main Sequence Stars from our color-magnitude diagram. I was helped a great by deal by Lee regarding all of these tasks.

Regarding the parts of the lab I did not focus on, first of all, I would like to thank Jim for writing the observing scripts and taking care of virtually all our observational needs. I would like to thank Lindsey and Jim for streamlining our image calibration software and making our bad pixel mask more robust. I would like to thank Lindsey, Christina, and Jim for writing our Photometry program using convolution. This program rivaled the mosaic programs in complexity, although I'd still say the ridiculousness award goes to the mosaic stuff, even though I am a bit biased. I would like to thank Christina for constructing the color-magnitude diagram which was quite useful near the end of the lab in estimating the age of the cluster. I would like to thank Amy and Jim for sharing their reports in progress, and Jim especially for a good discussion of the image calibration process, from flats, darks, sky, and bad pixels to the final calibrated data we threw into the mosaic program. I would also like to thank Jim for doing the majority of the error propagation. As always, I would like to thank James Graham and Nate McCrady for the continuous stream of helpful ideas. Nate gave me an extremely good explanation of how to think about color-color diagrams and reddening. And I would also like to thank John for getting such ridiculously good data, which we had a chance to feed through our mosaic program to produce some really fantastic color images. All in all, I'm sure I've left someone out, so thank you to all who I'm forgetting due to a slight case of not having slept in quite a while.

REFERENCES

1. Aspin et al. *"Near-IR Imaging Photometry of NGC 1333"*, Astron. Astrophys. Suppl. Ser. 106, 165-198 (1994)

2. Carroll Bradley W. and Ostlie, Dale A. *"An Introduction to Modern Astrophysics"*, Addison Wesley, 1996, pg.83, 212, and Appendix A13.

3. Huss, Lee. *"Near Infrared Observations of the Star Forming Region NGC 1333."* UC Berkeley Undergraduate Infrared Astronomy Laboratory, 11/13/2001.

4. Graham, James, *"An Infrared Camera for Leuschner Observatory and the Berkeley Undergraduate Astronomy Lab"*, Publications of the Astronomical Society of the Pacific, 113:607-621, 2001 May

5. Graham, James R., *ERRORS & STATISTICS: Ay 122 Lab Notes*, 2001

6. Graham, James R., *Lab 4 Handout*, 2001

7. Lada et al., *"Near Infrared Imaging of Embedded Clusters: NGC 1333"*, Astron. J. 111 (5), May 1996

8. Phillips, A.C. *"The Physics of Stars"* 2nd. ed. John Wiley & Sons, New York, 1999.

9. Taylor, John R., *An Introduction to Error Analysis.* University Science Books, Sausalito, CA 1997, 2nd ed.

10. Woan, G. *The Cambridge Handbook of Physics Formulas* Cambridge University Press, 2000. pg. 177